GSC Advanced Research and Reviews

eISSN: 2582-4597 CODEN (USA): GARRC2

Cross Ref DOI: 10.30574/gscarr

Journal homepage: https://gsconlinepress.com/journals/gscarr/

(RESEARCH ARTICLE)

Check for updates

EOR of heavy oil polymer on Alaska's North Slope: History matching challenges and solutions in a significant long-term water cut reduction

Shane Scott Namie * and Dongmei Wang

University of North Dakota Harold Hamm School of Geology and Geological Engineering of University of North Dakota Leonard Hall, Room 313 81 Cornell Street, Stop-8358 Grand Forks, ND 58202 (United States).

GSC Advanced Research and Reviews, 2024, 18(02), 072–086

Publication history: Received on 22 December 2023; revised on 02 February 2024; accepted on 04 February 2024

Article DOI: https://doi.org/10.30574/gscarr.2024.18.2.0039

Abstract

In 2016, a pilot program in Alaska's Milne Point Field tested polymer flooding for heavy oil recovery. Using four wells in the Schrader Bluff reservoir, it aimed to assess its effectiveness in capturing heavy oil resources. Generally, polymer flooding can boost oil production by 10-15%, typically occurring 6-9 months after injection. However, in this case, it took over 24 months for a polymer breakthrough. The method proved highly effective, consistently reducing water content by over 40% and maintaining a low level below 20% for 18 months. Applying standard simulation methods, like history matching, became challenging due to this prolonged low water cut. The usual history-matching processes focus on relative permeability, permeability corrections, and skin effect modifications. Nevertheless, these alternatives proved ineffective. In response to the extended low water cut in Alaska's North Slope, a unique approach was suggested. This approach entails highlighting the low-end point (Krw) across multiple relative permeability curves and adjusting these values according to the water cut history. Additionally, the method takes into account permeability adjustments, Equation of State on analyzes of oil viscosity, *J*-function incorporation, and considers the potential for viscous fingering during the process. The pilot program displayed remarkable polymer flooding effectiveness, but its unique performance on the North Slope required a modified history-matching approach to simulate its success accurately.

Keywords: Heavy oil; Polymer flooding; Ultra-low water cut; Multiple relative curves with low endpoints of krw

1. Introduction

Many studies have been conducted on polymer flooding in light oil reservoirs; however, little research has been conducted on its application in heavy oil reservoirs regarding numerical simulations. The existing literature predominantly focuses on light oil reservoir field performance and laboratory investigations. Only a few studies have published numerical simulation history matches specifically for heavy oil reservoirs using polymer flooding [5][14][8][9]. These few published papers highlight different approaches for achieving accurate history matches by adjusting various input parameters, such as the slope of the relative permeability curve, endpoint tuning, formation permeability corrections, and skin effect modifications, irrespective of the machine learning methods employed [11].

Delaplace et al. [5] examined the effects of polymer flooding on the Pelican Lake reservoir in their study based on a polymer flood pilot conducted in 2005. The authors modified simulation models to introduce heterogeneity, leading to excellent history matches. Five optimizations were performed to analyze polymer behavior accurately. The first optimization involved introducing a log-normal permeability field with gradual deformations. This adjustment aimed to represent the reservoir's heterogeneity better. The second optimization involved introducing a stratified heterogeneous distribution within the porous media, which improved the history match results. The third optimization involved introducing heterogeneities along the well axes. This adjustment significantly improved the history match for polymer breakthrough time and water-cut. The fourth optimization involved applying a dual gradient of permeabilities

* Corresponding author: Shane Namie

along the North-South direction, which slightly improved the history match for the central producer. Finally, the fifth optimization used core sample data to match the reservoir's geological permeabilities. The researchers improved the accuracy of the history match and better represented the reservoir's characteristics by incorporating this data, resulting in a good history match. Delaplace et al. [5] concluded that future studies should consider local variations in permeability to enhance history-matching accuracy in polymer flooding applications.

Pandey et al. [14] evaluated various chemical flood processes using the STARS/CMG (thermal simulator) software. Initial attempts at polymer flood matching were made without interpolating relative permeability curves, which resulted in poor history matching. The authors adjusted the relative permeability curves by reducing the endpoint of S_{orw} to improve the history match and concluded that S_{orw} is directly affected by the polymer solution's viscoelastic properties. This finding aligns with similar arguments presented in other publications on polymer floods in Daqing [7][6][16].

Fabbri et al. [8] used experimental laboratory results and numerical studies to determine the relative permeabilities for a secondary polymer flood. The researchers assessed the potential for polymer flooding in an extra-heavy oil field with viscosities ranging from 2,000 to 7,000 cP. A unique approach used by the researchers was the vertical placement of the core holder in an X-ray bank, which allowed them to monitor the saturation within the inner core throughout the experimental timeframe. The viscosity of the polymer had to be recalculated to account for the solutions' non-Newtonian shear-thinning behavior. The simulation model was refined to include 300 cells along the core axis to capture the polymer's dispersion accurately. The authors observed a small amount of viscous fingering occurring ahead of the polymer front during the first stages of the process.

While the literature cited above demonstrates commendable history matching outcomes through diverse approaches for polymer flooding in either field or core flooding lab-scale models, there seems to be a dearth of published works detailing the processes required to match a substantial reduction in water fraction— at least to the best of the author's knowledge. Notably absent is research on achieving a history match for a fractional water drop persisting over an extended period in a heavy oil reservoir. This study elucidates the methodologies developed and employed to successfully attain a satisfactory history match for a fractional water drop lasting more than 24 months on Alaska's North Slope (ANS). Noteworthy is the absence of any published work on the ANS reservoir that incorporates multiple relative permeability curves with low-end points (Krw), integrates permeability differential adjustments in both horizontal and vertical directions, and characterizes and fine-tunes Equation of State Models, and addresses viscous fingering during the process.

1.1. Pilot Description and Current Polymer Performance

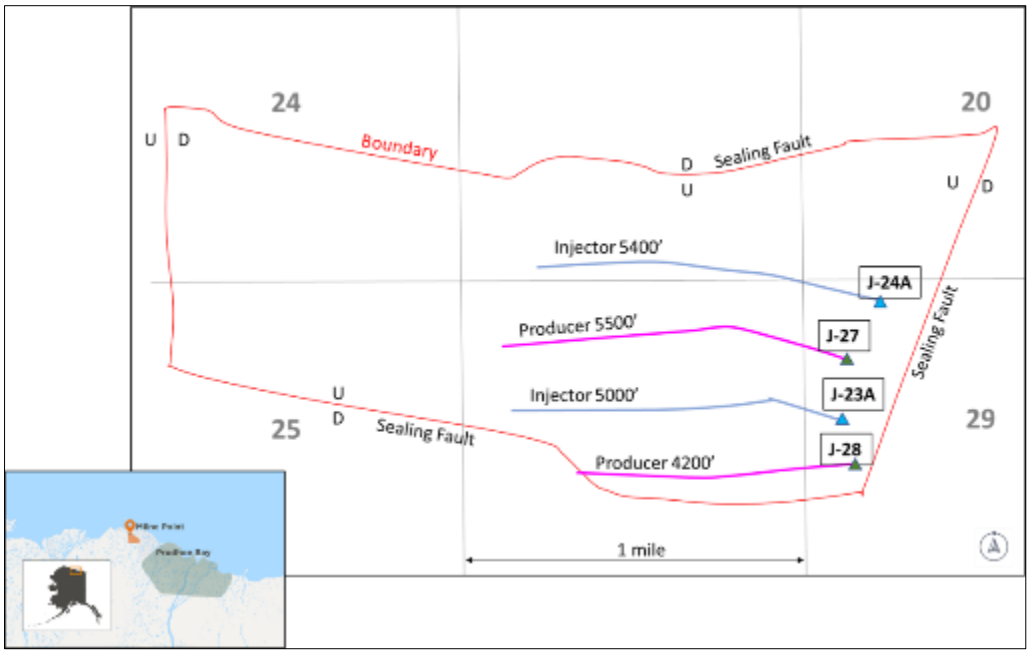

Figure 1 Polymer field pilot area boundary showing injector-producer well and pattern orientation [7]

Dandekar et al. [4] and Ning et al. [13] extensively describe the Milne Point Unit (MPU) located near Prudhoe Bay on the ANS. Two horizontal injection wells and two production wells were deployed within the Schrader Bluff reservoir on the

J-pad as part of the polymer flood pilot program [4]. The horizontal wellbores span between 1,280 to 1,676 meters (1,280 to 5,498.7 ft) in length, while the average distance between the well's measures approximately 376 meters (1,233.6 ft) (Fig.1). The Schrader Bluff reservoir within the Milne Point Unit (MPU) displays a range of porosity and permeability values, approximately 30-35% to 100-3,000 mD. The reservoir is characterized by a temperature of 21.1°C (70°F), the oil's API gravity measures approximately 15°, and has an in-situ oil viscosity of 300 cP [4].

Dandekar et al. [3] described that water flooding as a secondary recovery method resulted in recovery rates of 7.6% for oil and 67% for water prior to the polymer flood. Hydrolyzed polyacrylamide (HPAM) polymer injection began at the end of August 2018 to further enhance the recovery. The target viscosity for the injected polymer was set at 45 cP, with a polymer concentration ranging from 1,600 to 1,800 ppm; however, the polymer concentration was subsequently reduced to 1,200 ppm after some time due to injectivity issues, representing an injection volume of 0.12 pore volume (PV) up to the present [4].

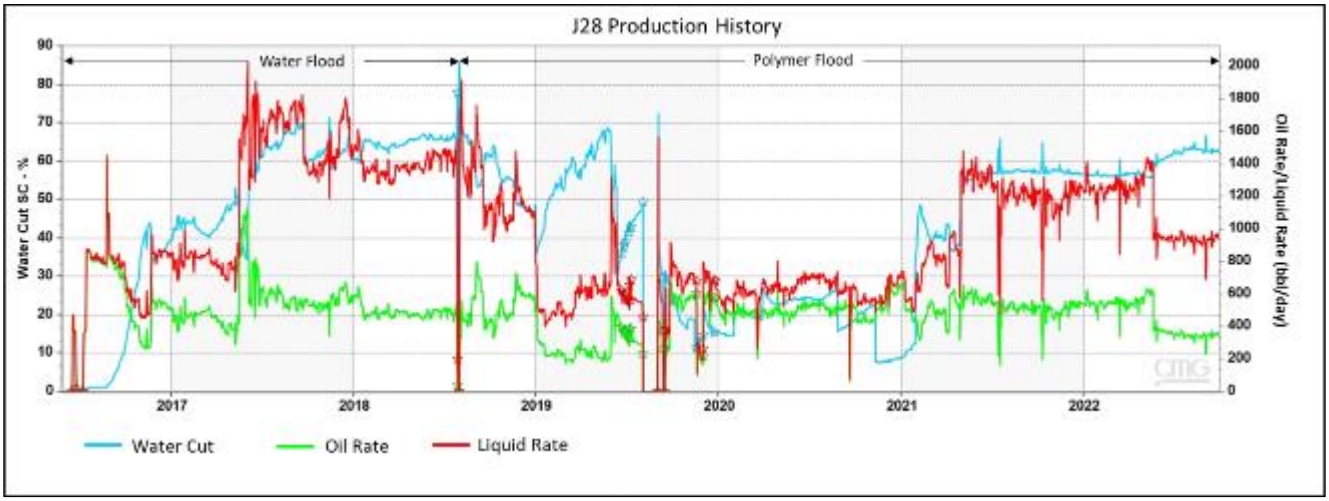

Figure 2 Well, J-28 production performance: May 2016 to Sept 2022

Fig. 2 illustrates the water cut trend at one of the producers, Well #J-28, from August 2018 to February 2021, exhibiting a notable decrease over time. This reduction in water cut indicates an enhanced sweep efficiency resulting from the polymer injection. The water cut peaked at 72.0% in September 2017 but steadily declined from 66.6% after polymer injection to 5.4% by February 2021. The data collected from the J-28 suggests that the oil production rate has stabilized since October 2019. Notably, the breakthrough of the polymer was observed in November 2021. Another producer, Well # J27 has similar production performance in water cut.

2. Numerical Simulation Model

Establishing the numerical simulation model for this study involved incorporating the various geological characteristics of the Milne Point field, such as seismic data, well logs, and wellbore trajectories. Laboratory analyses, including polymer rheology and other relevant laboratory studies, were integrated into the simulation model. The model also considered the reservoir system's petrophysical properties, such as subsurface porosity and permeability.

A numerical simulation was conducted using a corner coordinate system with an initial grid size of 193 x 221 cells and eight layers to represent the reservoir model accurately. The injection and production wells within the Schrader Bluff NB sand were within a fault block [4]; therefore, the model incorporated constraints on flow beyond these borders to maintain realistic boundaries (Fig. 3). This approach ensured that the simulation captured the specific conditions of the pilot project and provided a reliable representation of the reservoir's dynamics.

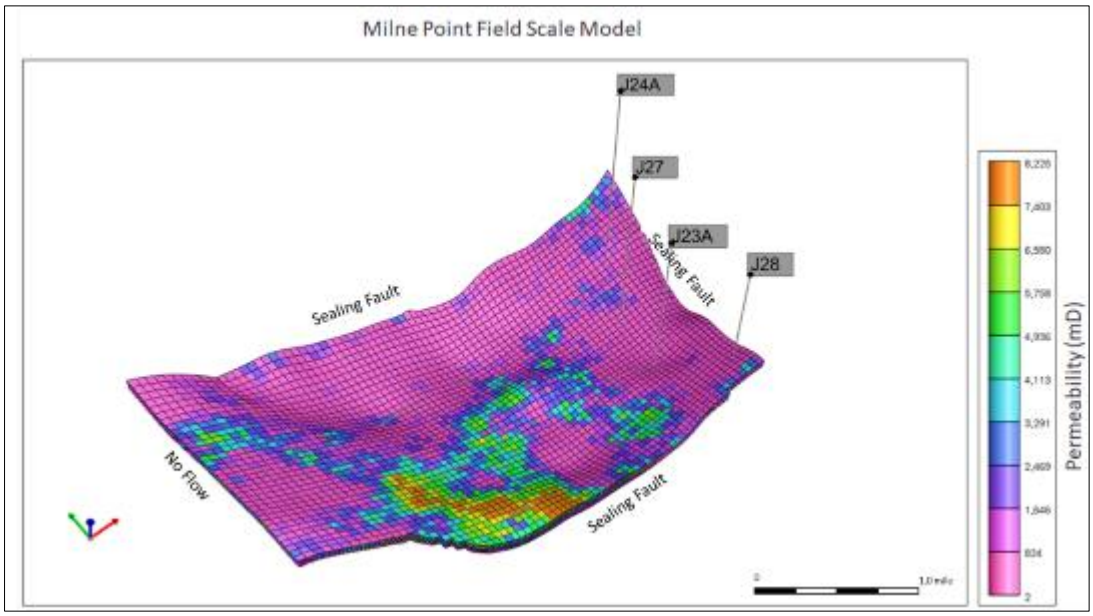

Figure 3 The grid top of the initial reservoir simulation model

A previous study of this research explored modern history-matching methods, including machine learning techniques such as CMG/CMOST [11]. This study focused on achieving a historic match between the field-scale model and production data. A lab-scale model was used to study the core flooding behavior before the field-scale production history match modeling was conducted. The field-scale model was developed based on the findings and parameters obtained. These methods are relevant to the broader context of the research and provide further insights into history-matching processes.

The field-scale numerical simulation model incorporated several vital parameters. The original formation water salinity was recorded at 27,000 ppm, while the salinity of the injection polymer solution was approximately 2,500 ppm. The reservoir temperature was maintained at 70°F throughout the simulation. The polymer had an initial molecular weight of 18×10^6 mDa and a viscosity of 45 cP. Adjustments were made to the polymer concentration and target viscosity after nearly two years of injection; the average polymer concentration was decreased from 1,800 ppm to 1,200 ppm, while the target viscosity was reduced from 45 cP to 30 cP. These modifications were based on observations and feedback from the field implementation. The field-scale model considered polymer rheology, including shear thinning and shear thickening at various flow rate conditions.

Afterward, the model incorporated polymer retention derived from field studies specific to the polymer flooding site and laboratory studies conducted explicitly for this purpose. Detailed polymer concentrations ranging from 500 ppm to 2,500 ppm were used to enhance simulation accuracy and closely align with production history instead of relying solely on average values over time. This adjustment enabled a more precise modeling approach by incorporating additional information on polymer concentrations as it became available. The simulation aimed to provide a more accurate representation of the polymer flooding process and its impact on production by considering the specific polymer retention characteristics and utilizing detailed concentration data.

The primary focus of the history matching process was aligning the water cuts and oil production rates in the two producing wells; therefore, the initial history match was conducted using constraints such as oil production rate, bottom-hole pressure, and water injection rate during the early stages of the polymer injection phase. Skin effect was also adjusted along with the above tunings.

Figure 2 illustrates the production performance following the polymer injection, exhibiting a rapid decrease in water cut, except for a temporary increase due to a workover. The water cut decreased from 60% (late October 2019) to 10% (beginning of February 2021) over 18 months. The water flooding history and traditional tuning methods, such as transmissibility and skin factor, failed to adequately explain the significant reduction in water-cut observed during the production history match despite the success of the initial relative permeability curve.

3. Methodology and Discussion

Methodologies for low-water cut history matches were integrated, and the following approaches are discussed below:

3.1. Endpoint of Water Relative Permeability Determination Through Various Overburden Pressures by Core Flooding

It is crucial to comprehensively understand the interactions between the rock and fluid to explain heavy oil production using the polymer process adequately. Accurately modeling and evaluating production mechanisms requires a thorough knowledge of the multiphase flow behaviors, particularly the relative permeability. For example, a study by Seright et. al [15], found that heavy oil reservoirs have a water permeability ranging from 0.05 to 0.15 at residual oil saturation; therefore, special attention was given to studying and acquiring the relative water permeability at residual oil saturations through laboratory experiments. A strong relationship exists between this information and an accurate representation of the flow behavior and optimization of the polymer flooding process for heavy oil reservoirs.

Theoretical considerations suggest that relative permeabilities are influenced by both external and internal applied stresses. For example, the in-situ stresses change when the reservoir undergoes water flooding. Pore pressure increases while the effective stress exerted on the rock mass decreases, and net pressure changes occur primarily due to changes in pore pressure rather than overburden pressure during production, water flooding, and polymer flooding operations [2]. These pressure changes can potentially impact fluid-fluid and fluid-rock interactions, ultimately modifying the shape of the relative permeability curves [2].

Some studies have used overburden pressure to simulate pore pressure and investigate the influence of effective pressure on relative permeability. For example, Jones et al. [10] explored how effective pressure affects relative permeability by subjecting samples to varying overburden pressures. The authors conducted laboratory experiments on core flooding, where overburden pressure was systematically adjusted to simulate reservoir permeabilities. Fig. 4 presents the outcomes obtained from targeted reservoir sands in the Milne Point field. The observations revealed a relationship between permeability and pore pressure, with a decrease in water-relative permeability as the applied pressure increased. These findings highlight the impact of pore pressure on permeability and emphasize the importance of considering pressure effects when examining relative permeability behavior.

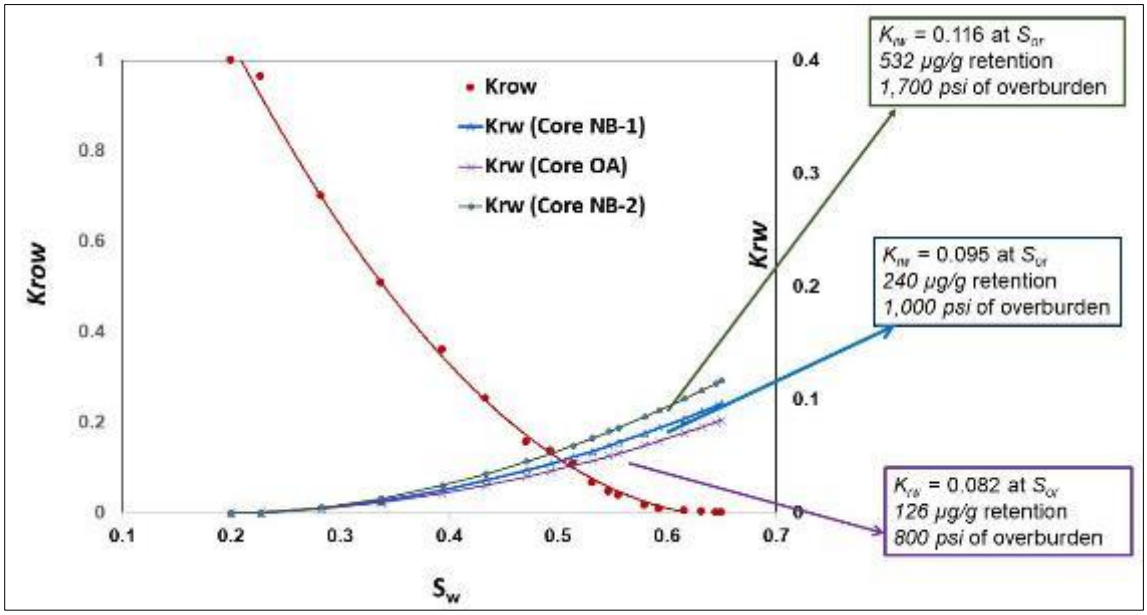

Figure 4 Relative water permeabilities were used for the core flooding simulations of the NB-1, NB2, and OA-1 sands

Increased pressure leads to a slight increase in the endpoint saturations, which was noted in previous studies [1][2], indicating that it is not unique to this particular case. Fig. 4 depicts three relative permeability curves, all generated using the same initial water saturation, residual oil saturation, and water saturation exponent (N_w). The relative permeability at each water saturation point is described by Equation 1:

$$k_{rw} = k_{rw}(endpoint\ at, S_{or})[S_{wn}]^{Nw} = k_{rw}(endpoint\ at\ S_{or})\left[\frac{S_w - S_{wi}}{1 - S_{wi} - S_{or}}\right]^{N_w} \ldots\ldots\ldots\ldots (1)$$

Where S_{wn} and S_w are normalized water saturation and local water saturation, respectively, N_w is Corey's water-saturation exponent, k_{rw} is the relative water permeability, and S_{wi} and S_{or} are initial water saturation and residual oil saturation, respectively. The k_{rw} at the endpoints were obtained by the ratio of k_w at the endpoints to the permeability of the core plugs. These relative permeability curves provide insights into the relationship between water saturation and relative permeability under varying pressure conditions. Changes in pressure can influence the relative permeability behavior, highlighting the importance of considering pressure effects when studying multiphase flow in reservoirs.

3.2. Vertical Permeability Adjustment

Understanding the relationship between vertical permeability (k_v) and horizontal permeability (k_h) in various types of sediment accumulation is crucial for comprehending oil reservoir production from a geological perspective. Primary production in a reservoir containing greywacke sediments yields low oil recovery with a big variance in k_v to k_h. In this type of sediment accumulation, the k_v is much lower than k_h [15]; however, this type of reservoir has exhibited promising results in terms of production during secondary or tertiary recovery processes. Furthermore, it indicates that the reservoir's response to enhanced oil recovery methods is significantly better than its performance under primary production alone.

The target reservoir may fall under the category of sediment accumulation characterized by heterogeneous permeability based on the nearly ten-month duration of the low water-cut stage observed in the Milne Point polymer project. There was a notable contrast between the vertical permeability (k_v) and the horizontal permeability (k_h), with the vertical permeability generally being much lower, resulting in significant variations in permeability over short distances within the reservoir. The prolonged low water-cut stage observed in the project provides evidence of the reservoir's heterogeneous permeability characteristics.

Adjusting the vertical permeability (k_v) and horizontal permeability (k_h) proportions accounts for permeability variations in sediment accumulation. The field-scale model incorporates multiple relative permeability curves considering different oil and water velocities. Fig. 5 presents the simulation results obtained by employing various permeability differentials, ranging from 0.1 to 0.7 (k_v:k_h). The graph illustrates that the best agreement with the water-cut history from Well #J-27, specifically during the low water-cut stage between mid-2019 and May 2020, is achieved when the k_v:k_h ratio is set to 0.25. The red curves in the figure represent this optimal scenario.

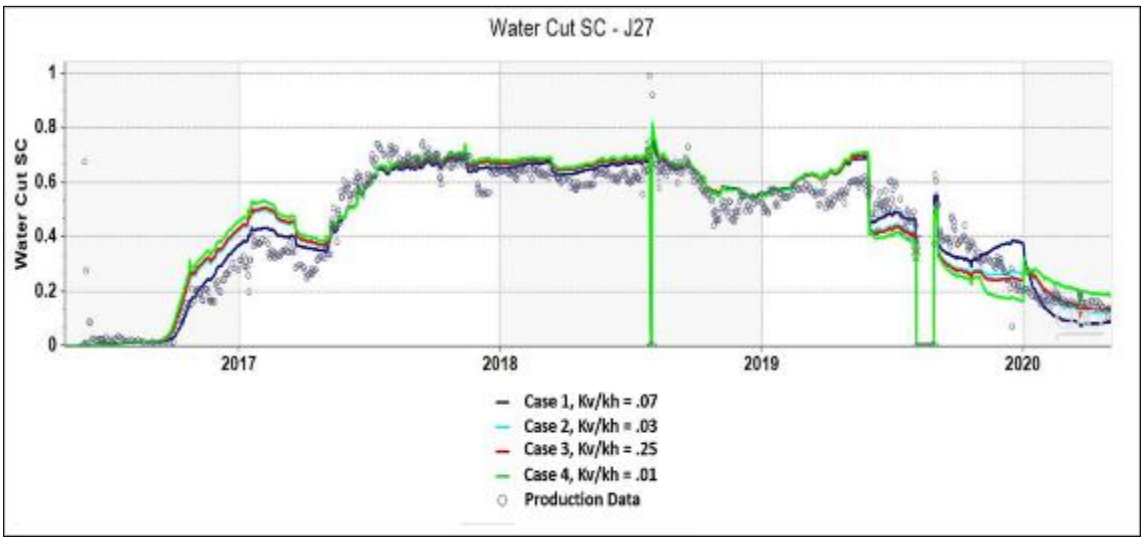

Figure 5 Water-cut history matches for #J-27 at various permeability differentials (k_v to k_h)

3.3. *J*-Function Incorporation

The *J*-function is also a crucial factor in understanding fluid distribution in porous media and fluid flow behavior driven by capillary forces; therefore, it is a valuable tool used in diverse subsurface applications, such as characterizing oil and

gas reservoirs, enhancing oil recovery, and optimizing water flooding operations. We gain valuable insights into fluid movement mechanisms and can improve the efficiency of fluid recovery processes by comprehending the *J*-function.

$$J(S_w) = \left(\frac{P_c(S_w)}{\sigma}\right)\left(\frac{k}{\phi}\right)^{1/2} \quad \text{..... (2)}$$

The *J*-function is expressed using various parameters, as Eq.2 shows, including water saturation (S_w), capillary pressure (P_c), permeability (k), porosity (ϕ), and interfacial tension (σ) between the two fluid phases. This study used a substantial *J*-function for eight relative permeability curves with various low endpoints in water (Fig. 6) to enhance the water-cut history match. The *J*-function was constructed based on capillary pressure measurements and other relevant reservoir parameters obtained from the Milne Point field. The accuracy of the water-cut history match was improved by incorporating this *J*-function, leading to a better understanding of the fluid behavior in the reservoir based on the vertical permeability differential adjustment.

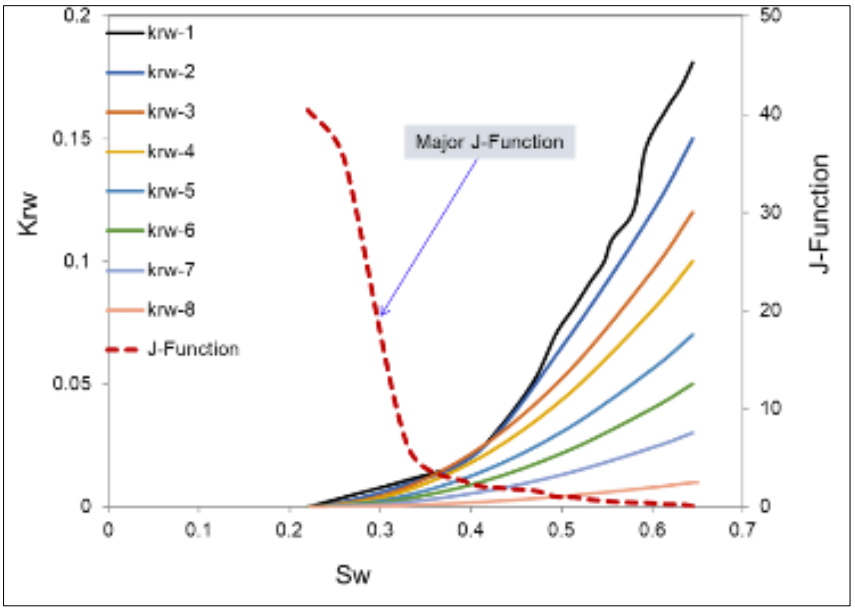

Figure 6 The *J*-function was used in the simulation

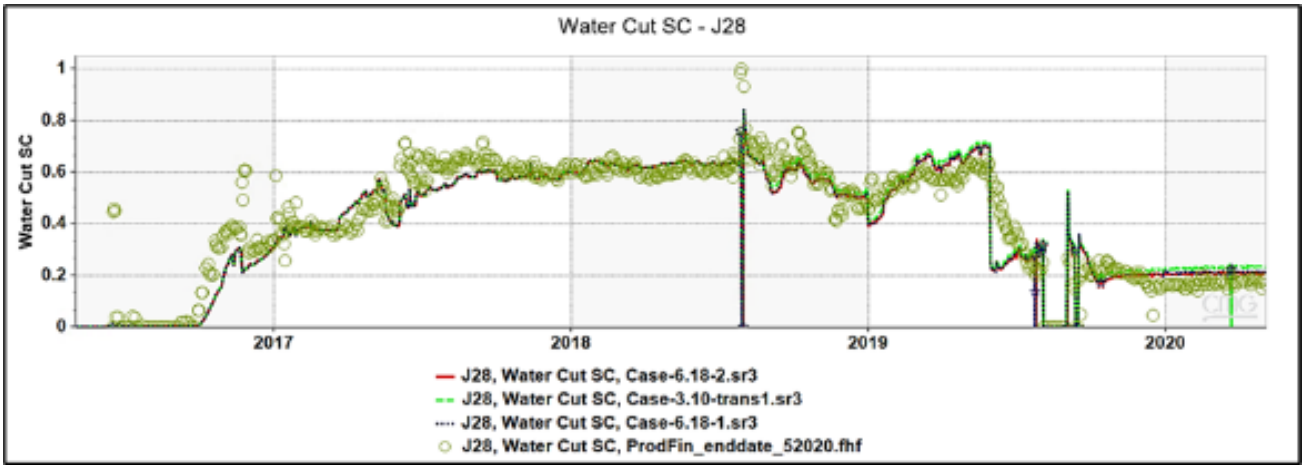

Figure 7 History matches # J-28 with the incorporated *J*-function

In addition, the lab-scale models were used to study how the shear effect affected *J*-function outcomes. The results obtained from the lab-scale model were initially compared with the calculated values (Fig. 7). After verification, the *J*-function plots were integrated into the long and low water-cut history match for Well #J-28.

Fig. 7 illustrates a better agreement in history matching vs. actual production after *J*-function incorporation. The green circle markers in Fig. 7 represent the actual water cuts obtained from production data, while the blue line illustrates the simulated result incorporating the shear effect for the case with an average permeability of 1,094 mD. The red line portrays the result containing the shear effect based on experimental laboratory findings. The remarkable agreement between the actual production data and the simulated results, which consider the shear effect, underscores the importance of accounting for this effect when calculating the *J*-function and understanding its impact on fluid flow within porous media.

3.4. Equation of State

The application of an equation of state (EOS) was initially introduced to predict phase behavior and characterize reservoir fluids during simulation. Accurately modeling the oil viscosity in heavy oil reservoirs was identified as a critical parameter in the EOS modeling process; therefore, the CMG/GEM (compositional simulator) field-scale model combined with CMG/IMEX (Black Oil Simulator) and STARS models was introduced to incorporate the heavy oil components in the target reservoir. Over 30 hydrocarbon components were combined into the GEM model, specifically categorized as '*Heavy*' and 'CH_4'. Here, the GEM, IMEX, and STARS are three modules of the Computer Modeling Group (CMG), which focus on different reservoir simulation functions.

Experimental data obtained from laboratory tests conducted by Hilcorp were compared with the EOS results to validate the accuracy of the oil viscosity modeling using the EOS. The EOS results (Figure 8a) demonstrated good agreement with the experimental data when the calculation involved only two lumped hydrocarbon compositions (Fig. 8a); however, slight differences from the experimental data were observed when ten hydrocarbon compositions, including N_2, H_2S, CH_4, and other components, were included in the calculation (Fig. 8b).

The production history matching for oil viscosity could have been improved by using only the EOS; if other parameter-matching results were incorporated into the component lumping process, specifically for the '*Heavy*' and 'CH_4' categories, following the EOS calculation. This approach resulted in a successful production history match for oil rates (Fig. 9 through 11). These results underscore the importance of considering multiple parameters and incorporating them into the EOS calculation to simulate heavy oil reservoirs accurately.

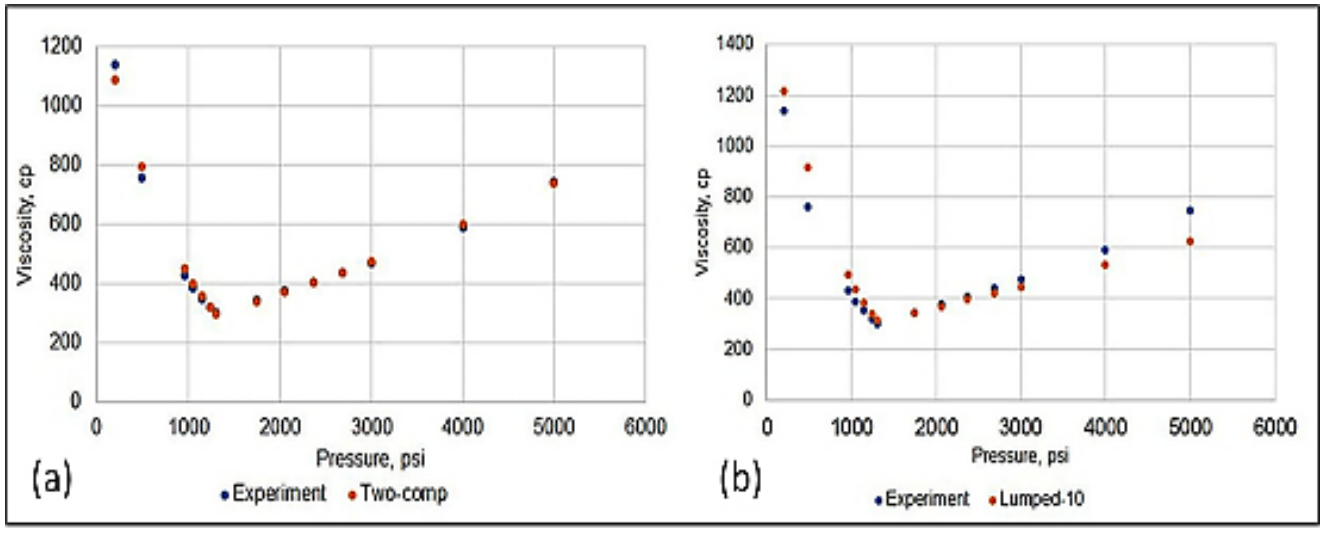

Figure 8 Oil viscosity calculations from EOS using different hydrocarbon composition lumping numbers: (a) two lumped hydrocarbon compositions and (b) ten hydrocarbon compositions

Furtherly, nineteen hydrocarbon components were incorporated in addition to the previously used compositions to enhance the EOS's calibration. The new components included N_2, CO_2, H_2S, C_1 *to* C_6, C_7-C_{10}, C_{11}-C_{16}, ….C_{132}-C_{200}, resulting in a better agreement (Fig. 9).

This comprehensive EOS modeling approach significantly improved the production history matching accuracy compared to the previous method, which used only two or ten hydrocarbon components. The results obtained from this calibration process were then used in subsequent simulation studies to enhance further the accuracy of predicting the heavy oil reservoir's phase behavior and fluid characteristics.

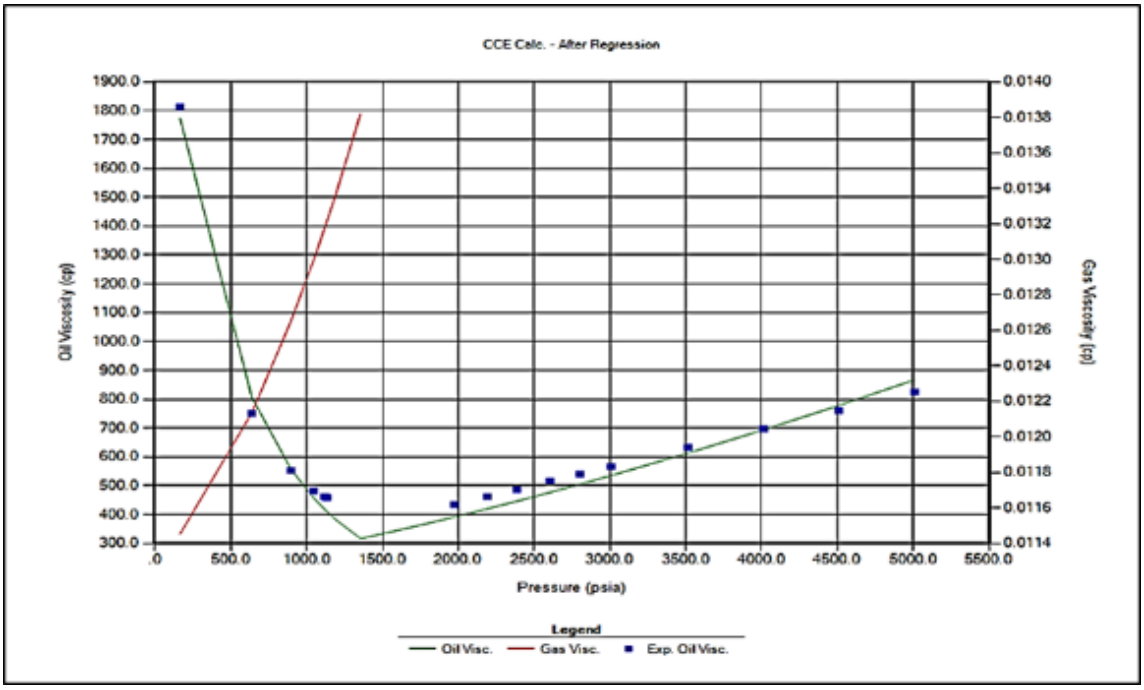

Figure 9 Regressed oil viscosity vs. pressure using the characterized heavy oil, with Pedersen as one reference model

Fig. 10 presents the history match results by August 2020 using the GEM with two EOS models for water cuts. The blue circles depict actual production data. The green and red lines represent the simulation results for two hydrocarbon components and 19 components in GEM.

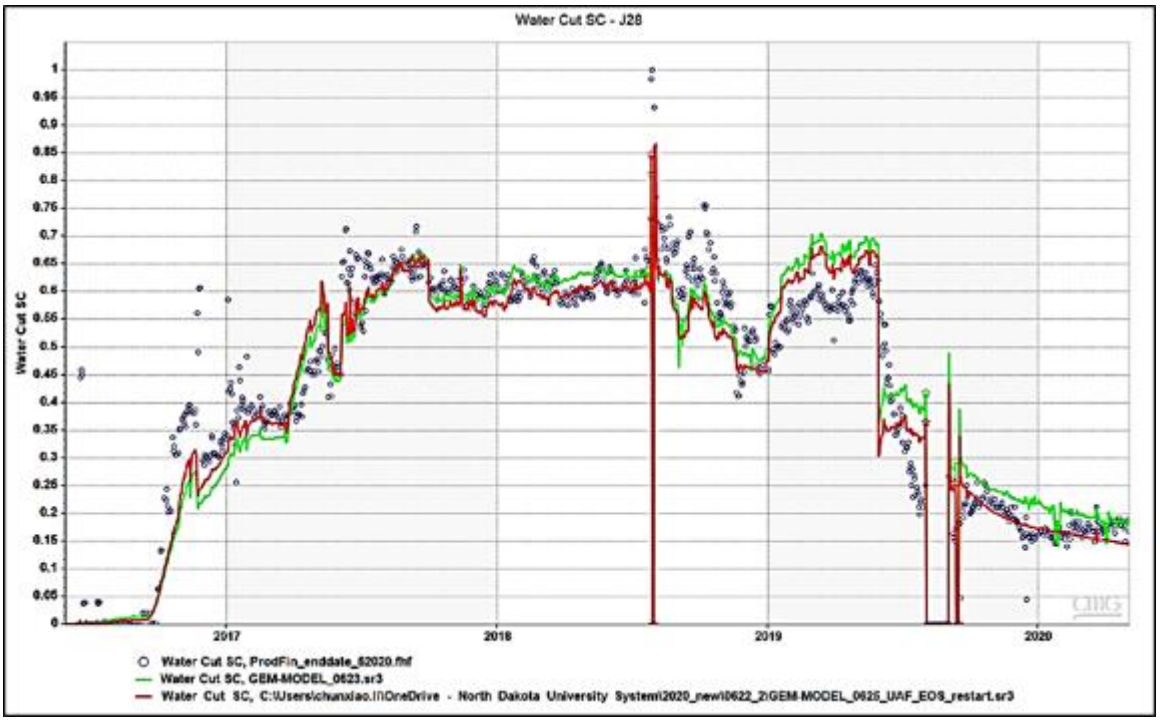

Figure 10 Water-cut history matches for well J-28

3.5. Viscous Fingering Number Consideration

The potential viscous fingering occurrence was considered in the study, and a viscous fingering number was calculated based on the research conducted by Zhang et al. [12] using the reservoir conditions and production data from the Milne Point field. These calculations were integrated into the field-scale model to achieve history matching. Fig. 11 illustrates

a water-cut simulation example for Well # J-28 after incorporating the effects of viscous fingering; however, there was room for further improvement in the agreement between the simulation results and the production data despite using a resolution value of 10E-8, which resulted in a basic match of the production data following experiments with CMG/CMOST (machine learning software). This limitation arose from the absence of provisions for dynamic resolution input and dynamic relative permeability curves in CMG; therefore, it was necessary to manually divide the permeability and velocity domains into different regions and perform manual simulations. Despite these efforts, a satisfactory history match for water cuts was not achieved in the later stage of 2019, leading to the decision to abandon incorporating the viscous fingering number.

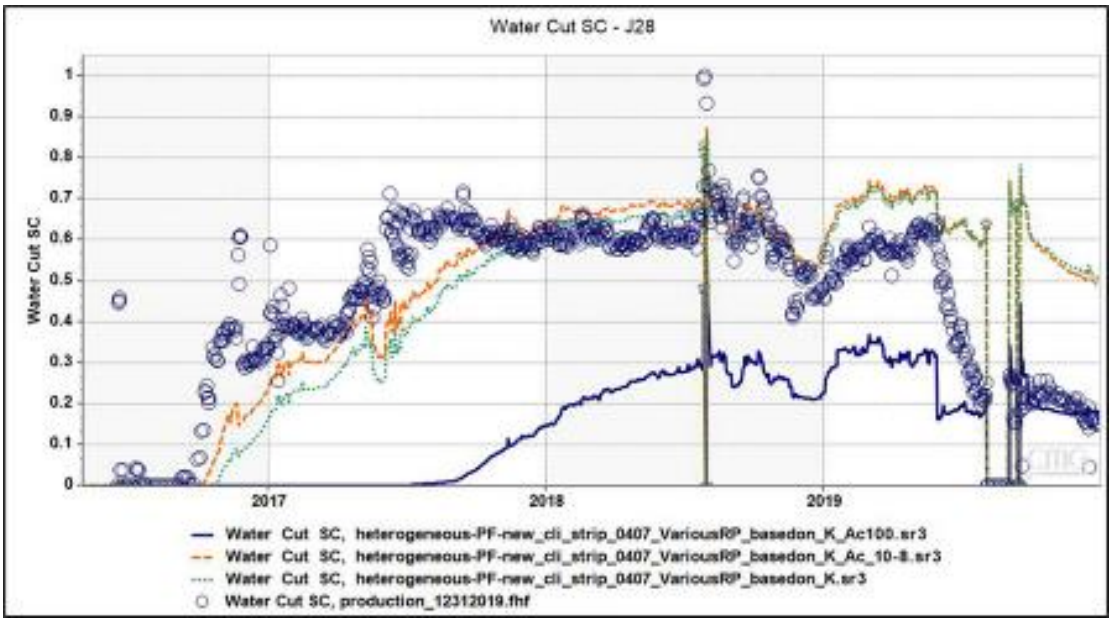

Figure 11 History matches with a viscous fingering model incorporated for Well #J-28

4. Multiple Relative Permeability Curves with Low Krw at Endpoints Application to Various Areas Near the Wellbores

The simulated production data initially exhibited a well-matched water-cut production history until mid-2019. The remarkable reduction in water-cut by the two producers, from 70% to 15%, is primarily attributed to this outcome. Besides the tunings using the methods above (vertical permeability adjustment, *J*-function incorporation, and EOS history matching), four additional water relative permeability curves were developed to achieve a satisfactory history match, including:

- CASE-1: The reservoir's original relative water permeability curve was modified by decreasing Krw's endpoint.
- CASE-2: The addition of a relative permeability curve for the region encompassing wells #J-28 and #J-23, and the area around Well # J-24, while retaining the original relative permeability curve for the area surrounding Well #J-27 (Fig. 12a). Here, the wells of J-23 and J-24 are the two injectors.
- CASE-3: Introduction of two more relative permeability curves for the near wellbores of J-24, J-23, J-28, and J-27 while using the original permeability curve for the remaining grid blocks in the simulation model (Fig. 12b).
- CASE-4: Multiple relative permeability curves are proposed for four large areas instead of using smaller regions (Fig. 13a, 13b, and 13c). This approach assumes that fluid flow changes predominantly occur within smaller regions rather than affecting the entire area; however, the original relative permeability curve remained in use for the area surrounding Well # J-27.

The endpoint of the lowest relative water permeability (K_{rw}) was gradually reduced to 1.2 times per order from the original water relative permeability curve, considering factors such as the actual extent of water cut reduction, laboratory studies (Fig. 4), and investigations of heavy oil relative permeability curves Seright et al. [15] Fig. 14 demonstrates a favorable agreement in the water-cut history match when these multiple curves are incorporated into the model.

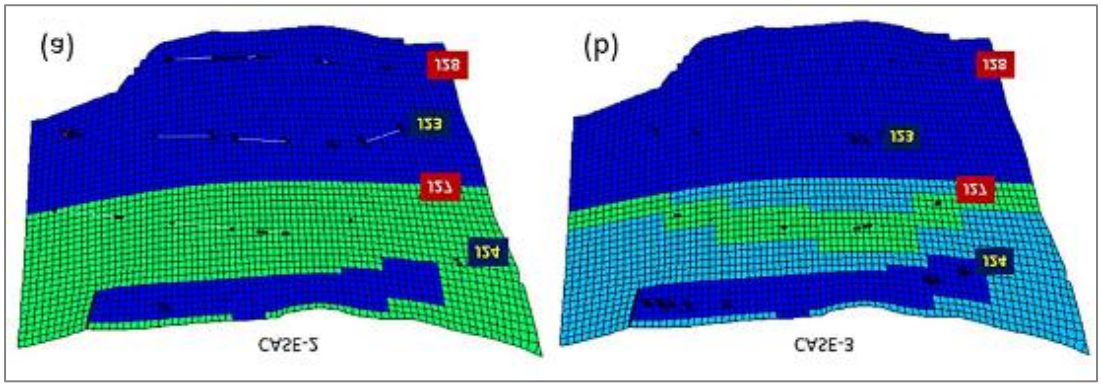

Figure 12 Areas corresponding to the different relative permeability curves

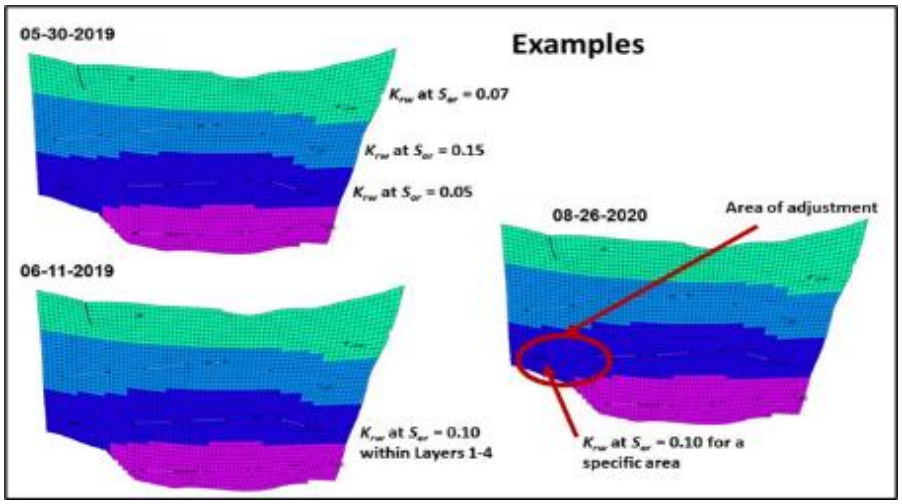

Figure 13 Multiple relative permeability curve applications in small regions

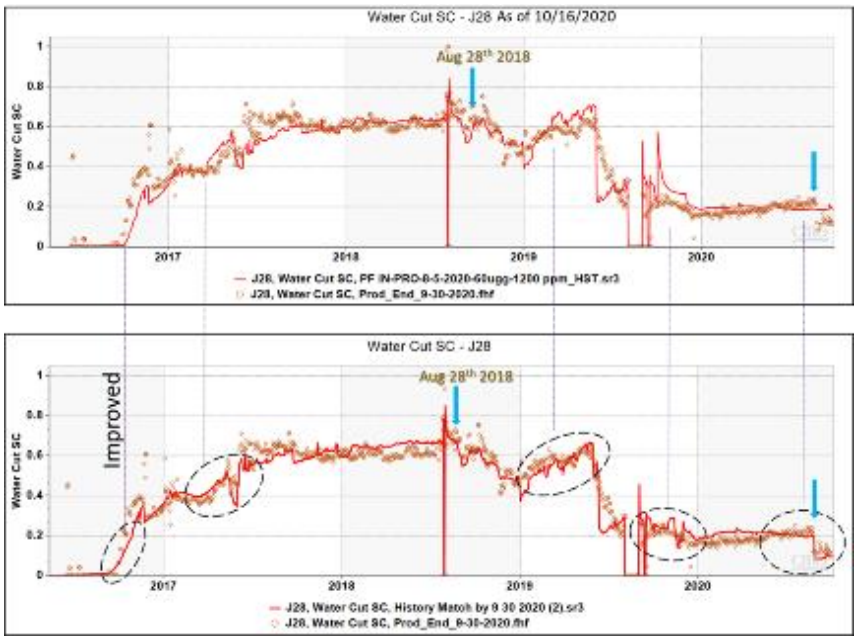

Figure 14 Water-cut history matches prior results (top) and improved outcomes (bottom)

5. Recent History Match Results

The most recent production data, as of the end of September 2022, comparing the history match is depicted in Fig. 15. There is a notable trend where the history match percentage consistently exceeds the production data percentage. This trend is evident from May 10, 2022, until the middle of June 2022. The history match percentage remains above 60% during this period, while the production data percentage fluctuates between 50% and 55%. Nevertheless, the history match for the pilot program provides a good fit.

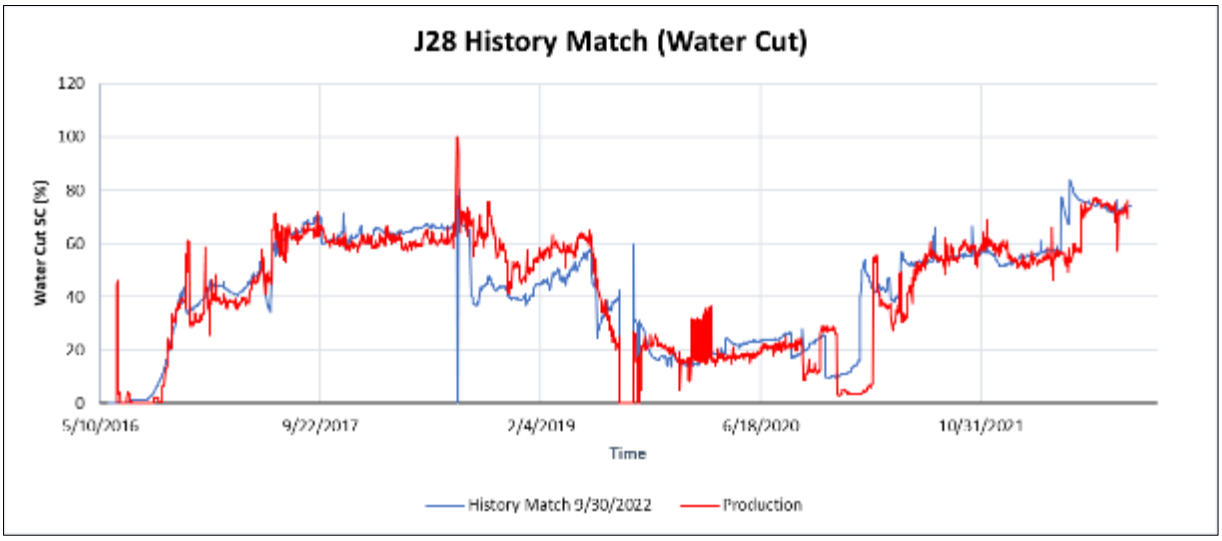

Figure 15 Water cut history match for Well #J-28

The oil recovery factor for water flooding was estimated to be 7.25% in early 2019 (Fig. 16), while it was projected to be 7.87% for polymer flooding. The difference between the two techniques was only 6.2%; however, the disparity between the two methods increased significantly as time progressed. The predicted oil recovery factor for water flooding was 20.22% after 21 years of injection (about 2 Pore Volume/PV), whereas polymer flooding was projected to reach 30.61%, indicating a polymer enhanced oil recovery of 10.39%.

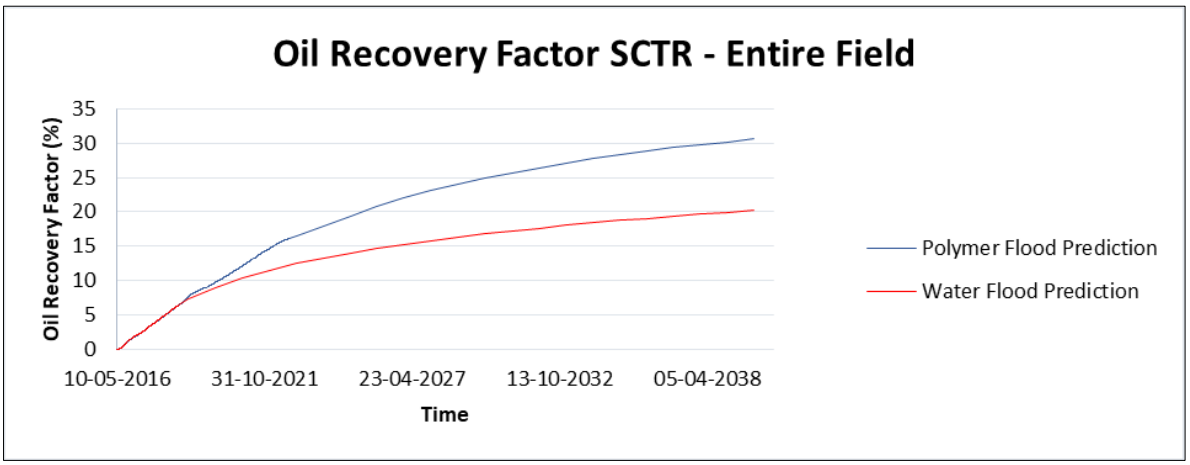

Figure 16 Oil recovery prediction results ending in 2040 indicate that the oil recovery factor for the polymer is significant

Polymer flood has a better sweep efficiency than water flood (Fig. 17). For example, water flood reached 90% of water cut at the beginning of 1/2024, whereas polymer flood is predicted to reach 90% pore volume as of 1/2040 based on a good history match. The final data from the pilot was analyzed and used to forecast the oil recovery factor, and water cut prediction through 2040. The data indicated that polymer flooding consistently resulted in higher oil recovery rates than water flooding. Polymer flooding also has better sweep efficiency than water flooding, suggesting that polymer flooding may be a more effective technique for oil recovery in the long term.

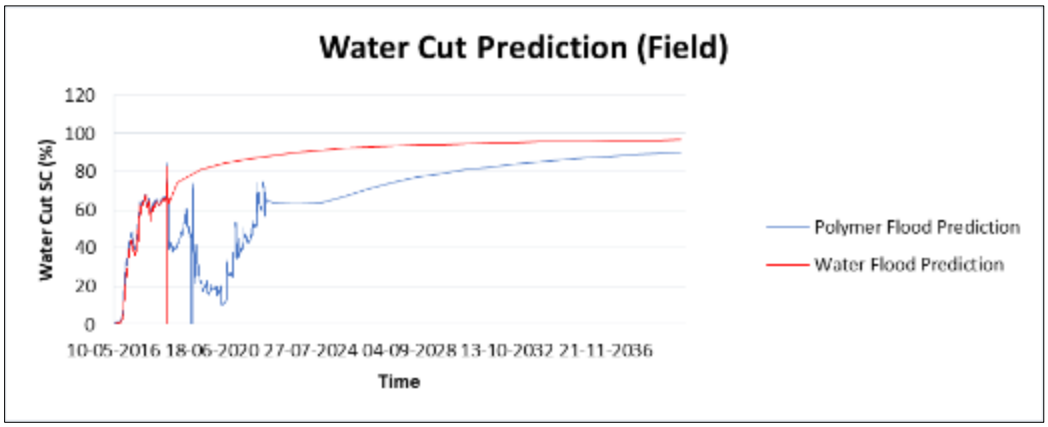

Figure 17 Water-cut predictions illustrate that the polymer has an increased sweep efficiency, reaching 90% pore volume by 1/2040

Nomenclature

ANS: Alaska North Slope
API: American Petroleum Institute
Bbl: Barrel
BHP: Bottom hole pressure
CMG: Computer Modeling Group
cP: Centipoise
EOR: Enhanced Oil Recovery
EOS: Equation of State
°F: Fahrenheit
Ft: Feet
K: permeability
$K_{h:}$ Horizontal permeability
Km: kilometer
$K_{rw:}$ Relative permeability of water in a two-phase oil-water system
$K_{v:}$ Vertical permeability
Md: millidarcy
mD: millidarcy
MPU: Milne Point Unit
$N_{w:}$ Corey exponent of water
Ppm: Parts per million
PV: Pore Volume
M: meter
$S_{wi:}$ Initial water saturation
$S_{or:}$ Residual oil saturation
$S_{orw:}$ Residual oil saturation to water
$K_{rw:}$ Relative water permeability
$K\gamma_{owm:}$ endpoint of oil relative permeability in oil-water displacement (at s_{grm})
$K\gamma_{wmax:}$ Endpoint of water relative permeability
$S_{org:}$ Residual oil saturation to gas
$S_{grm:}$ Gas saturation from which gas is mobile
$S_{wn:}$ Normalized water saturation
$S_{w:}$ Water saturation
Psi: Pound per square inch
$K_{ogi:}$ endpoint of oil relative permeability in gas-oil displacement (at S_{wi})
$K_{rgm:}$ Endpoint of gas relative permeability
Σ: Interfacial tension
Φ: porosity
$\sigma_{v:}$ Vertical applied stress
$\sigma_{H:}$ External Horizontal applied stress
$\sigma_{h:}$ Horizontal applied stress

P_c: Capillary pressure

SI Metric Conversion Factors

cp x 1.0*: E-03 = Pa・s
ft x 3.048*: E-01 = m
In. x 2.54*: E+00 = cm
md x 9.869 233: E-04 = μm2
psi x 6.894 757: E+00 = kPa
bbl x 1.589: E-01 = m3
°F (°F-32)/1/8: = °C
ft3 x 2.831 685E-02= m3

6. Conclusion

Conventional tuning methods failed to achieve a satisfactory history match for the sustained polymer performance during the extended low water-cut stage in the Milne Point heavy oil field; however, using the new method of multiple relative permeability curves with lower K_{rw} endpoints, including reducing the permeability proportions between k_v and k_h appropriate *J*-function, proved to be a practical approach for capturing the heterogeneity of the Milne Point field and obtaining a satisfactory history match for a long stage low water cuts. Incorporating multiple hydrocarbon compositions in the EOS flash calculations enhanced the accuracy of the numerical simulation.

Compliance with ethical standards

Acknowledgments

We thank Dr. Seright for providing the laboratory studies for this paper-associated content and the rest of the team associated with the Department of Energy Award Number DE-FE0031606 for exciting discussions.

We thank the Computer Modeling Group – CMG provides technical support for software utilization. "This material is based upon work supported by the Department of Energy under Award Number DE-FE0031606."

Disclaimer

Disclosure of conflict of interest

No conflict of interest to be disclosed.

References

[1] Ali HS, Al-Marhoun MA, Abu-Khamsin SA, Celik MS. The effect of overburden pressure on relative permeability. In: Middle East Oil Show. Society of Petroleum Engineers; 1987.

[2] Al-Quraishi A, Khairy M. Pore pressure versus confining pressure and their effect on oil–water relative permeability curves. J Petrol Sci Eng. 2005;48(1-2):120-126.

[3] Dandekar A, Zhang Y, Barnes J, Ning S, Seright R, Bai B, Wang D. First Ever Field Pilot On Alaska's North Slope to Validate the Use of Polymer Floods for Heavy Oil EOR. U.S. Department of Energy Office of Fossil Energy, Quarterly Research Performance Progress Report. 2020.

[4] Dandekar A, Zhang Y, Ning S, Seright R, Bai B, Wang D. DE-FE0031606-FINAL REPORT-June 1, 2018-October 31, 2022. United States. https://doi.org/10.2172/1916626. Accessed [date].

[5] Delaplace P, Delamaide E, Roggero F, Renard G. History matching of a successful polymer flood pilot in the Pelican Lake heavy oil field (Canada). In: SPE Annual Technical Conference and Exhibition. Society of Petroleum Engineers; 2013.

[6] Demin Q. Xiaohong, and Yang (2000). The Engineering and Technical Aspects of Polymer Flooding in Daqing Oil Field. 2000.

[7] Demin W, Gang W, Huifen X, Shuren Y, Wenxiang W. Incremental Recoveries in the Field of Large Scale High Viscous-Elastic Fluid Flooding are Double that of Conventional Polymer Flooding. In: SPE Annual Technical Conference and Exhibition. Society of Petroleum Engineers; 2011.

[8] Fabbri C, Romero C, Aubertin F, Nguyen M, Hourcq S, Hamon G. Secondary polymer flooding in extra-heavy oil: Gaining information on polymer-oil relative permeabilities. In: SPE Asia Pacific Enhanced Oil Recovery Conference. Society of Petroleum Engineers; 2013.

[9] Hatzignatiou DG, Norris UL, Stavland A. Core-scale simulation of polymer flow through porous media. J Petrol Sci Eng. 2013; 108:137-150.

[10] Jones C, Al-Quraishi AA, Somerville JM, Hamilton SA. Stress sensitivity of saturation and endpoint relative permeabilities. In: Paper SCA 2001-11 Presented at International Symposium of the Society of Core Analysts. 2001.

[11] Keith CD, Wang X, Zhang Y, Dandekar AY, Ning S, Wang D. Oil Recovery Prediction for Polymer Flood Field Test of Heavy Oil on Alaska North Slope Via Machine Assisted Reservoir Simulation. In: SPE Improved Oil Recovery Conference. One Petro; 2022.

[12] Luo X, Zhang L, Lei Y, Yang W. Petroleum migration and accumulation: Modeling and applications. AAPG Bull. 2020;104(11):2247-2265.

[13] Ning S, Barnes J, Edwards R, Dunford K, Eastham K, Dandekar A, et al. First Ever Polymer Flood Field Pilot to Enhance the Recovery of Heavy Oils on Alaska's North Slope—Polymer Injection Performance. In: Unconventional Resources Technology Conference, Denver, Colorado, 22-24 July 2019. Unconventional Resources Technology Conference (URTEC); Society of Exploration Geophysicists; 2019.

[14] Pandey A, Suresh Kumar M, Beliveau D, Corbishley DW. Chemical flood simulation of laboratory core floods for the Mangala field: generating parameters for field-scale simulation. In: SPE Symposium on Improved Oil Recovery. Society of Petroleum Engineers; 2008.

[15] Seright RS, Wang D, Lerner N, Nguyen A, Sabid J, Tochor R. Can 25-cp Polymer Solution Efficiently Displace 1,600-cp Oil during Polymer Flooding. SPE J. 2018;23(6). ISSN: 1930-0220. DOI:10.2118/190321-PA.

[16] Wang D, Seright RS, Shao Z, Wang J. Key aspects of project design for polymer flooding at the Daqing Oilfield. SPE Res Eval and Eng. 2008;11(06):1117-1124.